JCAMECH

Vol. 51, No. 2, December 2020, pp 417-431
DOI: 10.22059/jcamech.2020.308469.544

A refined inverse hyperbolic shear deformation theory for bending analysis of functionally graded porous plates

B. Sidda Reddy[a,] ∗ and K. Vijaya Kumar Reddy[b]

[a]*Rajeev Gandhi Memorial College of Engineering & Technology, Nandyal, Kurnool, A.P, India*
[b] *Jawaharlal Nehru Technological University, Hyderabad, Telangana, India*

ARTICLE INFO

Article history:
Received: 18 August 2020
Accepted: 03 September 2020

Keywords:
Functionally graded porous plates
Bending analysis
Rule of Mixtures
Porosity distribution
Porosity volume fraction

ABSTRACT

The modern engineering structures require the advanced engineering materials to resist the high temperatures and to provide high stiffness. In particular the functionally graded porous materials (FGPMs) introduced are expected to have these desired properties, consequently eliminating local stress concentration and de-lamination. In the present paper, a new shear strains shape function is chosen to research the bending analysis of functionally graded plates (FGPs) with uneven symmetrical, uneven asymmetrical and even distributions of porosity. The material properties of uneven porosity distributions along the thickness of the FGPs vary with cosine function. The present theory includes the influence of thickness stretching**.** This theory also fulfills the nullity of the shear stresses in the transverse direction on the top and bottom of the plate, thus avoids the use of a shear correction factor. The virtual displacement principle is employed to develop the equilibrium equations for porous FGPs. The Navier's method is used to obtain the solutions of porous FGPs for simply supported (SS) conditions. The accuracy of the developed theory is established with numerical results of perfect and porous FGPs available in the open source. The transverse displacements and stress results have been reported and studied for evenly, unevenly symmetrical and unevenly asymmetrical distributions with different porosity volume fraction (PVF), thickness ratios and aspect ratios. From the numerical results it is concluded that the type of porosity distribution needs to be considered as a key factor in the optimal design of the porous FGPs.

1. Introduction

The combined materials usage has been increasing day by day due to the lack of ability of conventional engineering materials to meet the desired properties demanded by the aerospace and other industries. These demanding properties can be achieved by employing the functionally graded materials (FGMs). These properties are attained by grading the physical properties in the thickness/length direction from one side to another side of the plate. Moreover, the porosity lowers the density and improves the stiffness of the structure. Hence, the materials with porosities have been extensively used in many fields of engineering like, aircraft, space vehicles, and military. Therefore, by coalescing the FGMs with porous materials, a novel material can be obtained which is known as porous FGMs [1-2]. These kinds of novel materials are produced by working with the pore coefficient and materials microstructure. Plates, shells and beams are the key elements in structural systems made of FGMs. The rectangular plates made with FGMs with porosities will have wide-ranging applications in the field of engineering. Therefore, it is important to investigate the bending analysis of FGPs with different kinds of porosities subjected to both sinusoidal loads (SSL) and uniformly distributed load (UDL) under simply supported boundary conditions.

In the past, many investigators contributed a lot in analyzing the static and dynamic behavior of perfect and porous FGPs. The vibration behavior of thin sector plates supporting on a Pasternak elastic foundation was analyzed by Mohammadi et al. [3] using a new differential quadrature method. These authors [4] also studied the effect of temperature change and in-plane pre-load on the vibration of circular and annular grapheme sheet embedded in a Visco-Pasternak foundation. Safarabadi et al. [5] used Gurtin-Murdoch model to investigate the surface effects on the vibration of rotating nano-beam. The influence of magnetic field, surface energy and compressive axial load on the dynamic and the

* Corresponding author. Tel.: +91-9440-844-0600; fax: +91-851-427-5123; e-mail: bsrrgmcet@gmail.com

stability behavior of nano-beam was investigated by Baghani et al. [6] using non local elasticity theory and the Gurtin Murdoch model. Goodarzi et al. [7], studied the effect of temperature on the vibration of FG circular and annular nano-plate embedded in a Visco-Pasternak foundation.

The elastic behavior of thick walled functionally graded spherical vessels under internal pressure was investigated by Zamani Nejad et al. [8]. These authors [9] also analyzed the ealsto-plastic deformations and stresses in FG rotating disk using elasto-perfectly-plastic material model. The effect of angular speed of the propagation of the plastic zone was studied and concluded that the density variation had a significant effect on the deformations and stresses. Mohammad Hosseini et al. [10-12] analyzed the stresses in a rotating functionally graded nano-disk subjected to thermo-mechanical loads using a strain gradient theory. Zeinab Mazarei and Mohammad Zamani Nejad [13] considered thick-walled functionally graded spherical vessel as thermo-elasto-plastic problem and analyzed by exposing the inner and outer surface to a uniform heat flux and an airstream respectively.

Mohammad Zamani Nejad et al. [14] used Frobenus series method to analyze the cylindrical pressure vessel for stresses. Mohammad Zamani Nejad et al. [15] provided an extensive literature review on the analysis of functionally graded thick cylindrical and conical shells by elastic theories, shear deformation theories, simplified theories and mixed theories. The effect of capture size in a spheroid living cell membrane under hydrostatic pressure was investigated by Hadi et al. [16] using strain gradient theory. Nejad et al. [17] analyzed the stresses in rotating functionally graded cylindrical pressure vessels under thermal load for purely elastic, partially plastic and fully plastic deformation condition by assuming the inner surface exposed to an airstream and the outer surface exposed to a uniform heat flux. The resonance behavior of Kirchhoff-three directional FG nano-plates were investigated by Behrouz Karami et al. [18]. The bi-Helmholz nonlocal strain gradient theory considered to capture the influence of small scale. Esmail Zarezadeh et al. [19] studied the influence of capture size in functionally graded nano-rod under magnetic field supported by a torsional foundation using nonlocal elasticity theory. To define the influence of torque of an axial magnetic field Maxwell's relation has been used.

The buckling response of nano-scale rectangular / circular plates made of graphene sheets was studied using the Galerkin method by Farajpour et al. [20-22] under different types of loading condition by considering the small scale effect. The first order shear deformation theory was used by Ghayour et al. [23] to examine the vibration of damped finite cylindrical shells in vacuum or in contact with interior/exterior dense acoustic media. Farajpour et al. [24] presented natural frequencies for nano-rings using the shear deformable ring theory by considering the small scale effect and concluded that the nonlocal effects should be considered in studying the vibrations. Danesh et al. [25] investigated the small scale effect on the axial vibration of the tapered nano - rod under different boundary conditions by employing the nonlocal elasticity theory and differential quadrature method. Ghayour et al. [26], Goodarzi et al. [27] and Mohammadi et al. [28] used the nonlocal elasticity theory and differential quadrature method to investigate the vibration behavior of orthotropic rectangular graphene sheet embedded in an elastic medium/ viscoelastic medium under biaxial pre load/ in-plane load.

The influence of temperature on the vibration of orthotropic rectangular/ annular nano plates made of nono-layer graphene sheet embedded in an elastic medium/Visco-Pasternak foundation was studied by Mohammadi et al. [29-31]. These authors also studied in the papers [32-33], the vibration behavior of circular and annular plates made of graphene sheets under in-plane pre-load and different boundary conditions using nonlocal elasticity theory and differential quadrature method. Asemi et al. [34] developed the nonlocal continuum plate model to study the transverse vibration of double-piezoelectric-nano-plate systems by employing the Pasternak foundation model with initial stress under an external electric voltage. The in-plane preload and small scale plays a significant effect on the resonance mode of smart nano structures. They also developed the nonlinear continuum model [35] to investigate the large amplitude vibration of nano-electro-mechanical resonators using piezoelectric nano-films under external electric voltage. Mohammadi et al. [36-37] used nonlocal elasticity theory to study the post buckling /shear buckling response of orthotropic single-layered graphene sheet. Farajpour et al. [38] investigated the influence of surface on the buckling behavior of microtubule systems in the visco-elastic surrounding cytoplasm using a modified Timoshenko beam model. These authors in [39] also investigated the vibration, buckling and smart control of microtubules embedded in an elastic medium in thermal environment using a piezoelectric nano shell. Asemi et al. [40] developed a nonlocal continuum model to investigate the piezoelectric nano films and double piezoelectric-nano-film systems.

Farajpour et al. [41] developed a nonlocal continuum model to study the nonlinear free vibration of size-dependent magneto-electro-elastic nano-plates under external electric and magnetic potentials. The influence of geometric nonlinearity was taken into account and the coupled nonlinear differential equations were solved using a perturbation technique. These authors also investigated in [42] the buckling of nano-plates resting on a two-parameter elastic foundation by developing the size-dependent plate model and in [43] the vibration of piezoelectric nano-films subjected to thermo-electro-mechanical loads using a higher order nonlocal strain gradient theory. The effect of humidity on the vibration frequencies of the rotating viscoelastic nano-beam embedded in the visco-Pasternak foundation under thermal environment was investigated by Mohammadi et al. [44].

Moslem Mohammadi and Abbas Rastgoo [45-46] carried out the experimental investigation of nonlinear free and forced vibration analysis of the sandwich nano-plates without and with considering porosity in the presence of the external harmonic excitation force. The foundation of the system was modeled by the nonlinear Pasternak foundation. The type of porosity distribution affects the mechanical behavior of the composite nano-plate. Mohammadi et al. [47] used nonlocal strain gradient elasticity theory to study the nonlinear free and forced vibration analysis of functionally graded nano-beam resting on a nonlinear foundation with porosity under mechanical and electrical loads. They found that length-scale parameters plays important role in the nonlinear vibration behavior of such structures. Sidda Reddy et al. [48-56] investigated the static bending subjected to mechanical and thermal load, inplane buckling and the free vibration behavior of perfect laminated composite and functionally graded plates with and without considering the thickness stretching using higher order shear deformation theory.

Many authors investigated on the free vibration and buckling behavior of FGPs with porosities (see Ref. [57-59].) In the last two years, only a few researchers investigated the flexural behavior of FGPs with porosities. The flexural behavior of FGPs with single layer and sandwich plate with porosities was investigated by Zenkour [57]. The plate was graded using

exponential and polynomial laws and primarily concentrated on sandwich plate. The influence of side to thickness ratios, aspect ratios, and exponents and porosity on the dimensionless deflections and stresses were examined.

Akbas [60] presented a Navier's solution to study the porosity influence and gradation index on the bending and the free vibration behavior of FGPs considering all sides are simply supported. The effective properties of the material such as modulus of elasticity and mass density were varied according to a power law distribution. The increase of porosity increases the dimensionless center deflections of the FG plate while it decreases the fundamental frequencies. Nguyen et al. [61] investigated the nonlinear response of FGPs using C^0 type higher order theory. In this, the two types of porosity models were considered along the thickness direction of the plate. The flexure, buckling and natural frequency behavior of nano FG porous plate's build-up with graphene platelets were studied by Li et al. [62]. Merdaci [63] analyzed the flexural response of rectangular FG plates with porosities by a higher order theory with four unknowns. The influence of exponent indexes in addition to porosity on the behavior of FGPs was also investigated. Demirhan and Taskin [64] used state-space approach to provide benchmark results to the bending and vibration of rectangular FGPs with porosity. Kim et al. [65-66] presented the numerical results of bending, vibration and buckling of FG porous micro plates. These plate theories were not satisfied the nullity conditions. Yang et al. [67] compared the bending solutions and the buckling response of different form of porous FG plates with a traditional sandwich plate. The effect of porosity and dimension ratios on stresses was also studied. The flexural behavior of FG sandwich plates with even, uneven, logarithmically uneven and linear-uneven porosities was investigated by Daikh et al. [68]. Amir Farzam and Behrooz Hassani [69] analyzed the static response of FG micro plates considering the porosities by employing Isogeometric analysis and modified couple stress theory. Sidda Reddy and Vijaya Kumar Reddy [70] investigated the effect of side to thickness ratio, aspect ratio, volume fraction of porosity, and type of porosity on the flexural behavior of functionally graded porous plates. In which, porosity is considered as a defect in manufacturing FG plate.

From the open source, and to the author's knowledge, it can be established the influence of thickness stretching needs to be considered to analyze the bending behavior of FG porous plates. These considerations are motivated to present the numerical results based on a novel higher order Quasi-3D theory to the bending response of FGPs with different forms of porosities considering the transverse extensibility along the thickness direction. This theory divides the transverse deflection into bending & shear components to see their contributions to the total transverse displacement. The present theory uses the novel higher order shear strain shape function that assesses the boundary conditions without restrictions on the upper and lower side of the FGPs in the absence of shear correction factors. The physical properties across the thickness of the FG plates with porosities are supposed to change with a cosine function while the Poisson's ratio keeps on constant. Navier solution is adopted to attain solutions for SS FGPs. The influence of side to thickness ratios, aspect ratios, and porosity distribution and also the volume fraction of porosity on the displacements and stresses are investigated in detail.

2. Formulation of novel higher order theory

Fig.1 represents a FG plate having physical dimensions and different kinds of porosity distributions with three dimensional Cartesian coordinate system. The plate made of FGM is subjected to bi-sinusoidal load q (x, y).

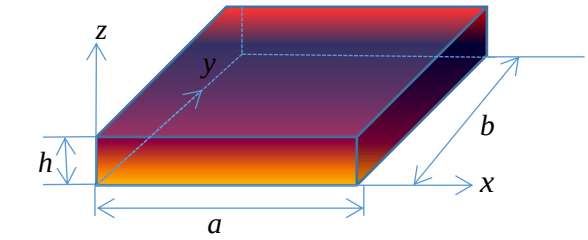

(a) Perfect FG Plate

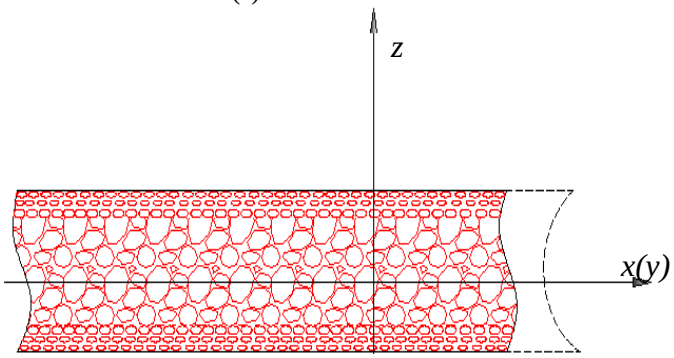

(b) Uneven symmetrical distribution

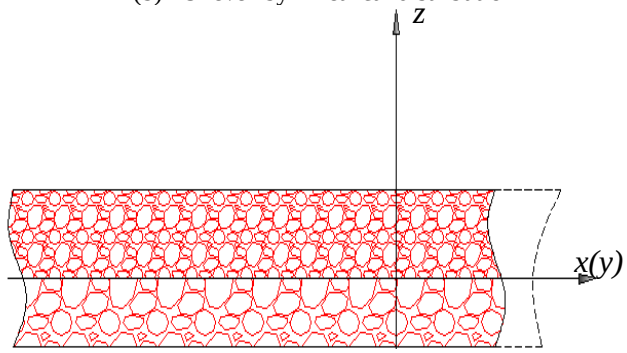

(c)Uneven asymmetrical distribution

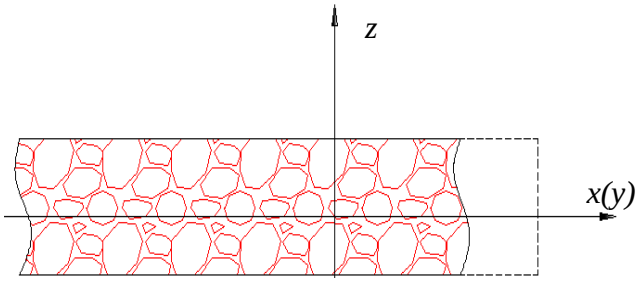

(d) Even distribution

Figure.1. Representation of FG rectangular plate with different kinds of Porosities [2]

The effective physical properties (P (z)) such as modulus of elasticity in tension, Young's modulus in shear and material mass along the thickness direction of the FG plates for three types of porosity distributions (Uneven symmetric distribution (USD), Uneven asymmetrical distribution (UAD) and Even distribution(ED) are expressed as [2]:

$$P(z) = P(1 - \mathrm{PVF} * \chi(z)) \qquad (1a)$$

$$\chi(z) = \begin{cases} \cos\left(\frac{\pi z}{h}\right) & \text{USD} \\ \cos\left(\frac{\pi z}{2h} + \frac{\pi}{4}\right) & \text{UAD} \\ \frac{1}{PVF}\left(1 - \left(\frac{2}{\pi}\sqrt{1-PVF} - \frac{2}{\pi} + 1\right)^2\right) & \text{ED} \end{cases} \quad (1b)$$

where, P is the property on the upper side of the plate & PVF is the porosity volume fraction.

Figures 2a-c depicts the variation of volume fraction of effective physical properties of the FG plates for three types of porosity models. In this, the volume fraction of effective physical properties is assessed using the Eq. (1) for different volume fraction of porosity (PVF) = 0.1, 0.3, 0.5, 0.7 and 0.9.

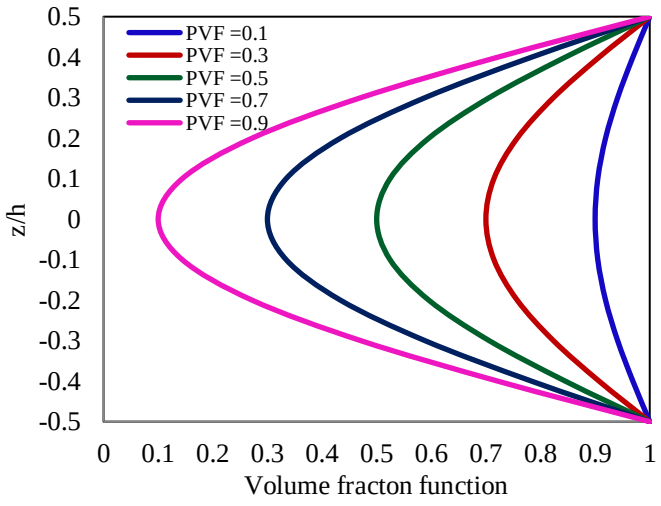

(a)

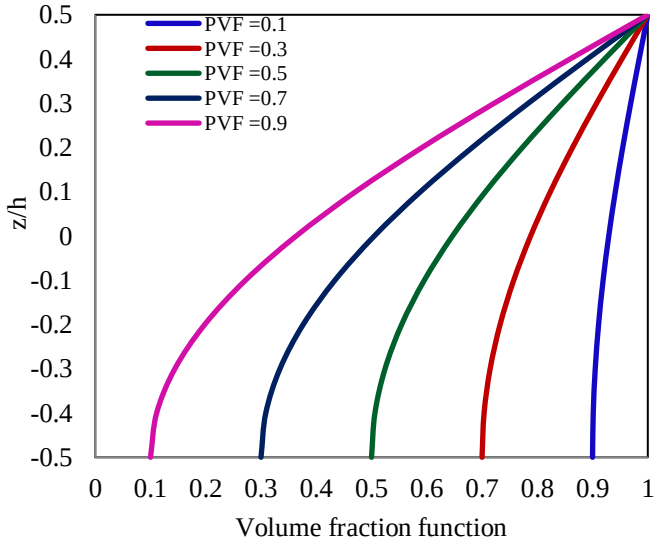

(b)

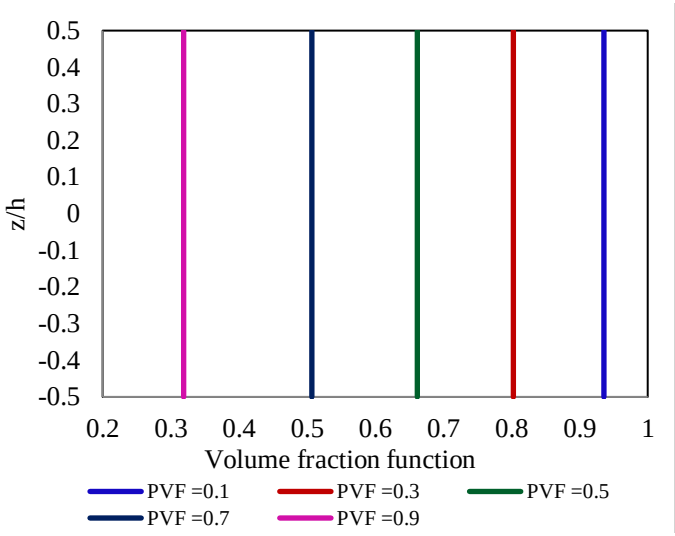

(c)

Figure. 2. Volume fraction variation along the thickness of the FG plate for various values of PVF for (a) Uneven symmetrical distribution; (b) Uneven asymmetric distribution; (c) Evenly distribution.

From Figure 2a, it can be seen that the volume fraction of physical property of the uneven symmetrical distribution is the minimum at the plate center and maximum at the upper and lower side of the plate. Also, the volume fraction of physical property decreases with the increase of PVF. In case of uneven asymmetrical porosity distribution, volume fraction of physical property decreases along the thickness direction from top to bottom with the increase of PVF (see Figure 2b), whereas in even porosity distribution, the volume fraction of physical property remains constant in the direction of thickness and decreases with the increase of the PVF (see Figure 2c).

2.1. Novelty of the Present Theory

(i) The normal and transverse shear deformations contribute significantly in accurately estimating the structural behavior of FG plates. Hence this theory considers the influence of normal and transverse shear deformations.

(ii) The displacement in the x and y-direction comprises extension, bending and shear components.

$$\bar{u}(x,y) = u - zw_{b,x} - \psi(z)w_{s,x} \quad (2a)$$

$$\bar{v}(x,y) = v - zw_{b,y} - \psi(z)w_{s,y} \quad (2b)$$

$$\text{Where } \psi(z) = z - \varsigma(z) \quad (2c)$$

$$\varsigma(z) = -\frac{8z^3}{3h^3\sqrt{1+2\pi^2}} + \text{Sinh}^{-1}\left(\frac{\sqrt{2}z}{h\pi}\right) \quad (2d)$$

The comma followed by the subscripts represents differentiation with respect to the subscripts throughout the paper. Equations (2c-d) represents the novel higher order shear strain function that satisfies the nullity conditions of the transverse stress at the top and bottom side of the plate. Thus, this theory doesn't require the shear correction factor.

(iii) The displacement in transverse direction w contains the bending (w_b), shear (w_s) and through the thickness stretching (w_t). The bending and shear parts are functions of x and y coordinates and the thickness stretching part is a function of x, y and z.

$$\bar{w} = w_b + w_s + \varsigma(z)_{,z}\xi \quad (2e)$$

ξ takes account of influence of normal stress.

(iv) The present theory involves only five unknown parameters.

2.2. Strain-displacement equations

The necessary relations are derived by assuming the strains are small. The strain displacement relations associated with the displacement model of Eqs. (2a-e), can be applied for thick to thin plates are as follows.

$$\epsilon_{11} = u_{,x} - zw_{b,xx} - \psi(z)w_{s,xx} \quad (3a)$$

$$\epsilon_{22} = v_{,y} - zw_{b,yy} - \psi(z)w_{s,yy} \quad (3b)$$

$$\epsilon_{33} = \varsigma(z)_{,zz}\,\xi \quad (3c)$$

$$\epsilon_{12} = (u_{,y} + v_{,x}) - 2zw_{b,xy} - 2\psi(z)w_{s,xy} \quad (3d)$$

$$\epsilon_{13} = \varsigma(z)_{,z}(w_{s,x} + \xi_{,x}) \quad (3e)$$

$$\epsilon_{23} = \varsigma(z)_{,z}(w_{s,y} + \xi_{,y}) \quad (3f)$$

2.3. Stress-strain relations

The linear stress-strain relations are given as:

$$s_{11} = Q_{11}\epsilon_{11} + Q_{12}(\epsilon_{22} + \epsilon_{33}) \quad (4a)$$

$$s_{22} = Q_{11}\epsilon_{22} + Q_{12}(\epsilon_{11} + \epsilon_{33}) \quad (4b)$$

$$s_{33} = Q_{11}\epsilon_{33} + Q_{12}(\epsilon_{11} + \epsilon_{22}) \quad (4c)$$

$$(s_{12}, s_{13}, s_{23}) = Q_{66}(\epsilon_{12}, \epsilon_{13}, \epsilon_{23}) \quad (4d)$$

In which, $s = \{s_{11}, s_{22}, s_{33}, s_{12}, s_{13}, s_{23}\}$ are the stresses and $\epsilon = \{\epsilon_{11}, \epsilon_{22,} \epsilon_{33}, \epsilon_{12}, \epsilon_{13}, \epsilon_{23}\}$ are the strains with regard to the coordinating system adopted for the plate and

$$Q_{11} = \frac{E(z)(1-\mu)}{(1-2\mu)(1+\mu)} \quad (4e)$$

$$Q_{12} = \frac{\mu E(z)}{(1-2\mu)(1+\mu)} \quad (4f)$$

$$Q_{66} = \frac{E(z)}{2(1+\mu)} \quad (4g)$$

2.4. Equilibrium Equations of motion

The static equations of equilibrium can be obtained by considering the virtual work and expressed in analytic form as

$$\int_x \int_y \int_z [s_{11}\epsilon_{11} + s_{22}\epsilon_{22} + s_{33}\epsilon_{33} + s_{12}\epsilon_{12} + s_{13}\epsilon_{13} + s_{23}\epsilon_{23}]\,dxdydz - \int_x \int_y q\left[\delta w_b + \delta w_s + \varsigma(z)_{,z}|^{h/2}\xi\right]dxdy = 0 \quad (5)$$

or

$$\int_x \int_y [N_1\,\delta u_{,x} - M_1\delta w_{b,xx} - P_1\delta w_{s,xx} + N_2\delta v_{,y} - M_2\delta w_{b,yy} - P_2\delta w_{s,yy} + S_3\delta\xi + N_6(\delta u_{,y} + \delta v_{,x}) - 2M_6\delta w_{b,xy} - 2P_6\delta w_{s,xy} + Q_{13}\left(\delta w_{s,x} + \delta\xi_{,x}\right) + Q_{23}\left(\delta w_{s,y} + \delta\xi_{,y}\right) - q\left(\delta w_b + \delta w_s + \varsigma(z)_{,z}|_{-h/2}^{h/2}\xi\right)]dxdy = 0 \quad (6)$$

In which N_i, M_i, P_i, S_i, Q_i denotes the forces and moment results which can be defined as follows

$$(N_i, M_i, P_i) = \int_{-h/2}^{h/2} S_{ij}\left(1, z, \psi(z)\right)dz, \quad (i,j = 1,2,6) \quad (7a)$$

$$S_3 = \int_{-h/2}^{h/2} S_{33}\,\varsigma(z)_{,zz}\,dz \quad (7b)$$

$$Q_{j3} = \int_{-h/2}^{h/2} S_{j3}\,\varsigma(z)_{,z}\,dz \quad (7c)$$

The equations of equilibrium are obtained from Eq. (6) by applying the integration by parts to the gradients of displacements and putting the coefficients of δu, δv, δw_b, δw_s and $\delta\xi$ to zero, independently. So, according to this theory, we have

$$\delta u = N_{1,x} + N_{6,y} = 0 \quad (8a)$$

$$\delta v = N_{2,y} + N_{6,x} = 0 \quad (8b)$$

$$\delta w_b = M_{1,xx} + M_{2,yy} + 2M_{6,xy} = -q \quad (8c)$$

$$\delta w_s = P_{1,xx} + P_{2,yy} + 2P_{6,xy} + Q_{13,x} + Q_{23,y} = -q \quad (8d)$$

$$\delta\xi = Q_{13,x} + Q_{23,y} - S_3 = 0 \quad (8e)$$

By putting Eq. (4a-g) into the Eq. (7a-c), and further substitution of the resulting equations into Eq. (8a-e) gives the system of equations in an abbreviated form as:

$$[\Theta]_{5\times5}[\Delta]_{5\times1} = [F]_{5\times1} \quad (9)$$

Where $[\Theta]$ contains stiffness terms and $\{\Delta\} = \{u, v, w_b, w_s, \xi\}^t$ denotes the unknown amplitudes and $\{F\} = \{0, 0, -q, -q, 0\}^t$ is the force matrix.

3. Analytical solution

In what follows, the solution for the Eq. (9) is obtained by prescribing the simply supported conditions at all the side edges:

$$N_1, M_1, P_1, v, w_b, w_s, w_{b,y}, w_{s,y}, \xi = 0 \;@\; x = 0,\; a.$$

$$N_2, M_2, P_2, u, w_b, w_s, w_{b,x}, w_{s,x}, \xi = 0 \;@\; y = 0,\; b. \quad (10)$$

In accordance with Navier's solution, the external transverse bi-sinusoidal load can be given as:

$$\mathrm{q(x,y)} = q_{kl}sin(\varphi x)sin(\phi y),\ (k,l = 1,2,\ldots.\infty) \quad (11)$$

Where $\varphi = \frac{k\pi}{a}$, $\phi = \frac{l\pi}{b}$, k and l are the mode numbers. For uniformly distributed, q_{kl} can be defined as:

$$q_{kl} = \begin{cases} \frac{16q}{kl\pi^2}, & \text{for odd k and l} \\ 0, & \text{otherwise} \end{cases} \quad (12)$$

In accordance with Navier's method, the assumed expressions for solutions that satisfy the SS conditions at all the side edges are

$$\mathrm{u(x,y)} = u_{kl}cos(\varphi x)sin(\phi y)$$

$$\mathrm{v(x,y)} = v_{kl}sin(\varphi x)cos(\phi y)$$

$$[w_b,\ w_s,\ \xi\ ] = [w_{bkl}, w_{skl}, \xi_{kl}]sin(\varphi x)sin(\phi y),\ (k,l = 1,2,\ldots.\infty) \quad (13a\text{-}c)$$

Where u_{kl}, v_{kl}, w_{bkl}, w_{skl}, ξ_{kl} are the unknowns to be determined.

Substitution of Eqs. (13a-c) into Eqs.(8a-e), the following system of equations in the first order is obtained.

$$[\bar{\Theta}]_{5\times5}[\bar{\Delta}]_{5\times1} = [\bar{\mathrm{F}}]_{5\times1} \quad (14)$$

Where

$$\Theta_{11} = -(A_{11}\varphi^2 + A_{66}\phi^2)$$

$$\Theta_{12} = -(A_{12} + A_{66})\varphi\phi$$

$$\Theta_{13} = B_{11}\varphi^3 + (B_{12} + 2B_{66})\varphi\phi^2$$

$$\Theta_{14} = B_{11}^S\varphi^3 + (B_{12}^S + 2B_{66}^S)\varphi\phi^2$$

$$\Theta_{14} = E_{11}\varphi$$

$$\Theta_{22} = -(A_{66}\varphi^2 + A_{11}\phi^2)$$

$$\Theta_{23} = B_{11}\phi^3 + (B_{12} + 2B_{66})\phi\varphi^2$$

$$\Theta_{24} = B_{11}^S\phi^3 + (B_{12}^S + 2B_{66}^S)\phi\varphi^2$$

$$\Theta_{25} = E_{12}\phi$$

$$\Theta_{33} = -D_{11}(\varphi^4 + \phi^4) - (2D_{12} + 4D_{66})\varphi^2\phi^2$$

$$\Theta_{34} = -D_{11}^{S}(\varphi^4 + \phi^4) - (2D_{12}^{S} + 4D_{66}^{S})\varphi^2\phi^2$$

$$\Theta_{35} = -G_{12}(\varphi^2 + \phi^2)$$

$$\Theta_{44} = -F_{11}(\varphi^4 + \phi^4) - (2F_{12} + 4F_{66})\varphi^2\phi^2 - L_{66}(\varphi^2 + \phi^2)$$

$$\Theta_{45} = -J_{12}(\varphi^2 + \phi^2) - L_{66}(\varphi^2 + \phi^2)$$

$$\Theta_{55} = -L_{66}(\varphi^2 + \phi^2) - K_{11}$$

Where $(A_{ij}|B_{ij}|D_{ij}|B_{ij}^{s}|D_{ij}^{s}|F_{ij}|E_{ij}|G_{ij}|J_{ij}|K_{ij}|L_{ij}) = \int_{-h/2}^{h/2} Q_{ij}(1|z|z^2|\psi(z)|z\psi(z)|\psi(z)^2|\varsigma(z)_{,zz}|z\varsigma(z)_{,zz}|\psi(z)\varsigma(z)_{,zz}|\varsigma(z)_{,zz}|\varsigma(z)_{,z}{}^2|\varsigma(z)_{,z}{}^2)dz$ $(i,j = 1,2,6)$

$$\{\bar{\Delta}\} = \{u_{kl}, v_{kl}, w_{b\,kl}, w_{s\,kl}, \xi_{kl}\}^t$$

$$\{\bar{F}\} = \{0, 0, -q_{kl}, -q_{kl}, 0\}^t$$

4. Results and Discussion

In the present paper, the results for the flexural response of simply supported porous FG rectangular plates are presented by applying SSL and UDL on the top side of the plate. The properties of materials used in the present paper are

Aluminium: Modulus of Elasticity (E_m)= 70 GPa, and Poisson's ratio (μ) are assumed as 0.3.

The displacements and stresses assessed here are presented using the following dimensionless forms:

$$W = w\left(\frac{a}{2}, \frac{b}{2}, z\right)\frac{10E_m h^3}{q_{kl}a^4}; S_{11} = s_{11}\left(\frac{a}{2}, \frac{b}{2}, z\right)\frac{h^2}{q_{kl}a^2};$$

$$S_{22} = s_{22}\left(\frac{a}{2}, \frac{b}{2}, z\right)\frac{h^2}{q_{kl}a^2}; S_{33} = s_{33}\left(\frac{a}{2}, \frac{b}{2}, z\right)\frac{h^2}{q_{kl}a^2};$$

$$S_{13} = s_{13}\left(0, \frac{b}{2}, z\right)\frac{h}{q_{kl}a} \qquad (15)$$

To validate the present theory results for dimensionless center plate deflections and normal stresses of exponentially graded plates, comparisons are made with: (i) 3-D exact solutions of the perfect plate [71]; (ii) Novel higher order theory, which includes new trigonometric shear strain shape function developed by Mantari and Guedes Soares [72] for perfect plate and (iii) recently a Quasi-3D refined theory developed by Zenkour [57] for single layer and sandwich plates with porosities.

Example 1: Considers transverse bi-sinusoidal load applied to the top of the rectangular/square plate. Tables 1 & 2 consists, results of dimensionless transverse center deflection *W* with and without inclusion of the porosity volume fraction and normal stress S_{22} of exponentially graded plates for various values of a/h, b/a ratios, and exponents ξ (for details Refer Zenkour [71]; Mantari and Guedes Soares [72]). The results estimated by the present theory are very close to the 3D exact solutions provided by Zenkour [71] and Mantari and Guedes Soares [72] results. Mantari and Guedes Sores [73] also provided over estimated results for dimensionless center plate deflection considering a trigonometric shape function in which the through the thickness stretching was neglected. So, the inclusion of through the thickness stretching is essential in estimating the dimensionless center deflections and stresses exactly.

Example 2: The dimensionless center deflections of simply supported perfect and FG plate with even & uneven porosity variation subject to UDL are given in Table 3. The reported results are compared to those presented by DEMIRHAN and TASKIN [64] based on sinusoidal shape function with $\epsilon_{33} = 0$. On the basis of numerical results, it is noticed that the through the thickness stretching has noteworthy on the deflections.

Lastly, additional results of dimensionless transverse center deflections, and stresses in rectangular FG porous plates with three kinds of distributions of porosity are reported in Tables 4-6. The increase of PVF increases the transverse deflection and axial stress, while it decreases the transverse shear stresses for both SSL & UDL. The reason is an increase in the PVF results in a decrease in the Young's modulus of the plate. The dimensionless deflections decrease with the increase of a/h, while it increases with increase of b/a.

The dimensionless center deflections are somewhat larger for even porosity distribution compared to uneven porosity distributions. We can affirm that the side-to-thickness ratio a/h, aspect ratio b/a, and PVF has a considerable effect on the deflections and stresses for the three types of distributions. The influence of shear component is to decrease the deflections with an increase of thickness ratios. It is because; the shear deformation is more noticeable in thick plates.

Figure 3 indicates the through-the-thickness variation of dimensionless deflections of rectangular FG plate for a/h=5 with several values of PVF for three types of porosity distributions. From Figures 3a-c it is seen that the deflection increases as PVF increases for both SSL and UDL. The maximum center deflection occurs at the plate center for all types of porosity distributions, porosity volume fractions and varies symmetrically about the mid plane along the thickness of the plate (see Figures. 3a-c). Also seen that for the even porosity distribution with UDL shows larger deflection compared to other two types of uneven porosity distribution values along the thickness direction for all porosity volume fractions.

The distribution of dimensionless axial stress S_{11} of thick (a/h=5) rectangular (b/a=3) FG plate in the thickness direction is portrayed in Figure 4 for several values of PVF. The axial stresses are tensile and compressive respectively at the top and bottom surface of the plate, for three types of porosity distributions and for all values of PVF. The increase of PVF results in increase of S_{11} for two types of uneven porosity distributions for both SSL and UDL. This can be defended by the reality that the porosity lessens the stiffness of the plate. Whereas for the even porosity distribution, S_{11} varies anti-symmetrically about the mid plate for all porosity volume fractions and for both SSL & UDL. Also, noticed that for even porosity distribution the stress S_{11} varies only in the thickness direction and is independent of PVF. From Figures. 4a-c it is noteworthy to see that the PVF of uneven symmetrical, uneven asymmetrical and evenly distribution has no influence on axial stress in three, two and one position respectively, are S_{11}=-0.6402 (UDL), -0.401(SSL) at z/h=-0.39, S_{11}=0 (SSL and UDL) at z/h=0, and S_{11}=0.4 (UDL), 0.64 (SSL) at z/h=0.39 & S_{11}=-0.4 (UDL), 0.24(SSL) at z/h=-0.28, and S_{11}=0.52 (UDL), 0.32 (SSL) at z/h=0.356 & S_{11}=0 (UDL and SSL) at z/h=0.

The variation of normal stress S_{33} in the thickness direction of very thick (a/h=5) rectangular (b/a=3) FG plate is shown in Figure 5 for several values of PVF. The normal stresses are tensile and compressive respectively, are at the upper and lower surface of the plate, for three types of porosity distributions and for all values of PVF. The PVF has no influence on normal stress S_{33} in three and one positions for uneven symmetrical and evenly distributions (see Figures 5a, 5c) respectively, are S_{33}=-0.02 (SSL), 0.037 (UDL) at z/h=0.41, S_{33}=0 (SSL& UDL) at z/h=0, S_{33}=0.02 (SSL), 0.032 (UDL) at z/h=0.41 & S_{11}=0 (UDL and SSL) at z/h=0. The effect of PVF in the thickness direction for uneven asymmetrical distribution is shown in Figure 5b.

Table 1: Dimensionless deflections of perfect and porous FG plate (SSL)

a/h	b/a	Theory	ξ=0.1	ξ=0.3	ξ=0.5	ξ=0.7	ξ=1.0	ξ=1.5
2	1	3-D [71]	0.57693	0.52473	0.47664	0.4324	0.37269	0.28904
		Mantari and Soares [72]	0.57789	0.5224	0.47179	0.42567	0.36485	0.27939
		Zenkour [57](PVF =0)	0.5751	0.5199	0.4695	0.4236	0.3624	0.2781
		Present	0.57760	0.52220	0.47160	0.42550	0.36400	0.27930
		Zenkour [57]((PVF=0.1)	0.7182	0.6493	0.5864	0.5291	0.4526	0.3473
		Present (PVF =0.1)	0.7214	0.6521	0.589	0.5314	0.4546	0.3488
	2	3-D [71]	1.19445	1.08593	0.9864	0.8952	0.77266	0.60174
		Mantari and Soares [72]	1.19408	1.07949	0.97503	0.8799	0.75377	0.57862
		Zenkour [57](PVF =0)	1.1909	1.0766	0.9725	0.8776	0.7512	0.5771
		Present	1.1938	1.0793	0.9748	0.8797	0.753	0.5785
		Zenkour [57]((PVF=0.1)	1.4873	1.3445	1.2145	1.096	0.9381	0.7208
		Present (PVF =0.1)	1.4909	1.3479	1.2174	1.0987	0.9403	0.7224
	3	3-D [71]	1.44295	1.3116	1.19129	1.08117	0.93337	0.7275
		Mantari and Soares [72]	1.4421	1.30373	1.17761	1.06279	0.91041	0.69925
		Zenkour [57](PVF =0)	1.4387	1.3007	1.1749	1.0604	0.9077	0.6977
		Present	1.4419	1.3035	1.1774	1.0626	0.9096	0.6991
		Zenkour [57]((PVF=0.1)	1.7968	1.6244	1.4673	1.3242	1.1336	0.8713
		Present (PVF =0.1)	1.8007	1.6279	1.4704	1.3271	1.136	0.8731
4	1	3-D [71]	0.349	0.31677	0.28747	0.26083	0.22534	0.18054
		Mantari and Soares [72]	0.3486	0.31519	0.28477	0.2571	0.22028	0.1697
		Zenkour [57](PVF =0)	0.3481	0.3148	0.2844	0.2568	0.22	0.1695
		Present	0.3486	0.3152	0.2848	0.2571	0.2203	0.1697
		Zenkour [57]((PVF=0.1)	0.4348	0.3931	0.3552	0.3207	0.2748	0.2117
		Present (PVF =0.1)	0.4353	0.3936	0.3556	0.3211	0.2751	0.212
	2	3-D [71]	0.81529	0.73946	0.67075	0.60846	0.52574	0.412
		Mantari and Soares [72]	0.81448	0.73647	0.66547	0.60093	0.51508	0.39732
		Zenkour [57](PVF =0)	0.8135	0.7357	0.6648	0.6003	0.5146	0.3969
		Present	0.8145	0.7365	0.6655	0.6009	0.5151	0.3973
		Zenkour [57]((PVF=0.1)	1.0161	0.9187	0.8302	0.7497	0.6426	0.4957
		Present (PVF =0.1)	1.0172	0.9197	0.8311	0.7505	0.6433	0.4962
	3	3-D [71]	1.01338	0.91899	0.8335	0.75606	0.65329	0.51209
		Mantari and Soares [72]	1.01243	0.91546	0.82724	0.74704	0.64037	0.49408
		Zenkour [57](PVF =0)	1.0113	0.9145	0.8264	0.7463	0.6397	0.4936
		Present	1.0124	0.9155	0.8272	0.747	0.6404	0.4941
		Zenkour [57]((PVF=0.1)	1.2630	1.1421	1.032	0.932	0.7989	0.6164
		Present (PVF =0.1)	1.2644	1.1433	1.0331	0.9329	0.7997	0.617

Table 2: Dimensionless axial stress of perfect and porous FG plate (SSL)

a/h	b/a	Theory	ξ=0.1	ξ=0.3	ξ=0.5	ξ=0.7	ξ=1.0	ξ=1.5
2	1	3-D [71]	0.31032	0.32923	0.34953	0.37127	0.40675	0.47405
		Mantari and Soares [72]	0.29244	0.31468	0.33826	0.36325	0.40405	0.47848
		present	0.2927	0.3149	0.3386	0.3636	0.4039	0.479
	2	3-D [71]	0.31998	0.33849	0.35833	0.37956	0.41417	0.47989
		Mantari and Soares [72]	0.30422	0.32613	0.34945	0.37427	0.41483	0.49052
		present	0.3049	0.3269	0.3503	0.3752	0.4156	0.4918
	3	3-D [71]	0.30808	0.32525	0.34362	0.36329	0.39534	0.45619
		Mantari and Soares [72]	0.29122	0.31177	0.33369	0.35707	0.39537	0.46732
		present	0.2921	0.3127	0.3348	0.3582	0.3964	0.4689
	4	3-D [71]	0.30084	0.31727	0.33486	0.35368	0.38435	0.44257
		Mantari and Soares [72]	0.28335	0.30317	0.32431	0.3469	0.38394	0.45373
		present	0.2843	0.3042	0.3255	0.3481	0.3851	0.4554
4	1	3-D [71]	0.22472	0.23995	0.25621	0.27356	0.30177	0.35885
		Mantari and Soares [72]	0.22372	0.23907	0.25544	0.27291	0.30137	0.35555
		present	0.2244	0.2399	0.2563	0.2739	0.3024	0.3568
	2	3-D [71]	0.24314	0.25913	0.27618	0.29434	0.32385	0.37968
		Mantari and Soares [72]	0.23953	0.25497	0.27154	0.28936	0.3187	0.37562
		present	0.2408	0.2564	0.2731	0.291	0.3205	0.3777
	3	3-D [71]	0.23188	0.24692	0.26295	0.28002	0.30775	0.36021
		Mantari and Soares [72]	0.22721	0.24137	0.25663	0.27312	0.30044	0.35404
		present	0.2287	0.243	0.2584	0.275	0.3025	0.3565
	4	3-D [71]	0.2247	0.23918	0.2546	0.27103	0.2977	0.34816
		Mantari and Soares [72]	0.21957	0.23302	0.24754	0.26327	0.28943	0.34105
		present	0.2211	0.2347	0.2494	0.2652	0.2916	0.3436

Table 3: The dimensionless center deflection of perfect and porous FG square plates subjected to UDL

a/h	Exponent (ξ)	Method	ε_{33}	Even			Unevn		
				PVF					
				0	0.2	0.4	0	0.2	0.4
5	0	Ref. [64]	=0	0.5352	0.60706	0.70111	0.5352	0.58052	0.63466
		Present	≠ 0	0.5443	0.6175	0.7133	0.5443	0.5664	0.5909
	0.1	Ref. [64]	=0	0.58992	1.67969	0.80066	0.58992	0.64981	0.71393
		Present	≠ 0	0.5997	0.69	0.8126	0.5997	0.6263	0.6561
	0.5	Ref. [64]	=0	0.8083	0.98705	1.3267	0.8083	0.92411	1.08409
		Present	≠ 0	0.8124	1.0003	1.3145	0.8124	0.8644	0.9257
	1	Ref. [64]	=0	1.04469	1.43735	2.47062	1.04469	1.27236	1.66012
		Present	≠ 0	1.0371	1.4063	2.3506	1.0371	1.1339	1.2587
10	0	Ref. [64]	=0	0.46655	0.52922	0.61134	0.46655	0.5045	0.54923
		Present	≠ 0	0.477	0.5411	0.6251	0.477	0.4929	0.5101
	0.1	Ref. [64]	=0	0.51714	0.59566	0.89806	0.51714	0.56398	0.64537
		Present	≠ 0	0.5279	0.6079	0.7166	0.5279	0.5475	0.5688
	0.5	Ref. [64]	=0	0.71361	0.8895	1.18947	0.71361	0.81751	0.95489
		Present	≠ 0	0.7223	0.8931	1.1821	0.7223	0.763	0.8098
	1	Ref. [64]	=0	0.92873	1.29241	2.29216	0.92873	1.13392	0.8372
		Present	≠ 0	0.9234	1.2641	2.1611	0.9234	1.0019	1.1015
20	0	Ref. [64]	=0	0.44939	0.50971	0.5888	0.44939	0.48543	0.52782
		Present	≠ 0	0.46	0.5218	0.6028	0.46	0.4744	0.4897
	0.1	Ref. [64]	=0	0.49834	0.57412	0.67728	0.49834	0.54338	1.38928
		Present	≠ 0	0.5097	0.5871	0.6923	0.5097	0.5276	0.5467
	0.5	Ref. [64]	=0	0.69209	0.86177	1.1551	0.69209	0.79069	0.92626
		Present	≠ 0	0.6995	0.8661	1.1487	0.6995	0.7373	0.7806
	1	Ref. [64]	=0	0.89968	1.25611	2.2436	0.89968	1.09915	1.44418
		Present	≠ 0	0.8946	1.2282	2.1132	0.8946	0.9685	1.0618

Table 4: Influence of thickness ratio, aspect ratio, porosity distribution and porosity volume fraction on Dimensionless center defection in FG plate

a/h	b/a	Distribution	PVF =0.1		PVF =0.3		PVF =0.5		PVF =0.7		PVF =0.9	
			SSL	UDL	SSL	UDL	SSL	UDL	SSL	UDL	SSL	UDL
2	1	USD	0.6484	1.0511	0.7535	1.2216	0.9096	1.4745	1.1735	1.9024	1.7497	2.8366
		UAD	0.6487	1.0517	0.7536	1.2217	0.9059	1.4686	1.1542	1.8711	1.6849	2.7315
		ED	0.6491	1.0523	0.7566	1.2265	0.9177	1.4878	1.1979	1.942	1.9048	3.0879
	2	USD	1.332	2.1594	1.5255	2.4731	1.806	2.9278	2.2677	3.6762	3.2484	5.2661
		UAD	1.3392	2.1711	1.5528	2.5173	1.8651	3.0236	2.3843	3.8653	3.5543	5.762
		ED	1.3412	2.1742	1.5632	2.5341	1.8962	3.074	2.4751	4.0124	3.9355	6.38
	3	USD	1.6064	2.6041	1.8332	2.9718	2.1595	3.5009	2.6924	4.3648	3.8144	6.1837
		UAD	1.617	2.6214	1.874	3.038	2.2505	3.6484	2.8795	4.6681	4.3146	6.9946
		ED	1.6197	2.6258	1.8878	3.0605	2.29	3.7124	2.9892	4.8458	4.753	7.7052
	4	USD	1.7261	2.7982	1.9671	3.189	2.313	3.7498	2.876	4.6625	4.0572	6.5772
		UAD	1.7383	2.8181	2.0142	3.2654	2.4188	3.9212	3.0958	5.0188	4.6477	7.5345
		ED	1.7414	2.8231	2.0297	3.2903	2.462	3.9913	3.2137	5.2098	5.11	8.284
5	1	USD	0.3514	0.5697	0.3887	0.6301	0.4379	0.7099	0.5096	0.8262	0.6402	1.0379
		UAD	0.3574	0.5793	0.4125	0.6688	0.4948	0.8021	0.6379	1.0342	0.9981	1.6181
		ED	0.3584	0.5811	0.4178	0.6772	0.5068	0.8215	0.6615	1.0723	1.0518	1.7051
	2	USD	0.8418	1.3647	0.9241	1.4981	1.0296	1.6691	1.1765	1.9072	1.4246	2.3094
		UAD	0.858	1.391	0.9896	1.6043	1.1866	1.9237	1.5327	2.4847	2.4217	3.9258
		ED	0.8613	1.3964	1.0039	1.6275	1.2178	1.9742	1.5896	2.5769	2.5275	4.0975
	3	USD	1.0518	1.7051	1.1529	1.869	1.2816	2.0777	1.4588	2.3649	1.7525	2.8411
		UAD	1.0726	1.7388	1.2368	2.0051	1.483	2.4041	1.9162	3.1064	3.0335	4.9177
		ED	1.0769	1.7458	1.2552	2.0348	1.5225	2.4683	1.9874	3.2218	3.1601	5.1229
	4	USD	1.145	1.8562	1.2544	2.0336	1.3933	2.2588	1.5838	2.5675	1.8972	3.0756
		UAD	1.1678	1.8932	1.3466	2.183	1.6146	2.6174	2.0865	3.3825	3.3054	5.3584
		ED	1.1726	1.901	1.3667	2.2156	1.6579	2.6877	2.164	3.5082	3.441	5.5783
10	1	USD	0.3061	0.4962	0.3331	0.54	0.3663	0.5938	0.4091	0.6632	0.4721	0.7654
		UAD	0.3128	0.5071	0.3604	0.5843	0.432	0.7004	0.5592	0.9065	0.8934	1.4483
		ED	0.314	0.509	0.3659	0.5933	0.4439	0.7196	0.5794	0.9393	0.9213	1.4936
	2	USD	0.7689	1.2464	0.8348	1.3533	0.9145	1.4826	1.0149	1.6454	1.1544	1.8715
		UAD	0.7864	1.2749	0.9058	1.4685	1.0857	1.7601	1.4061	2.2795	2.2533	3.653
		ED	0.7899	1.2805	0.9207	1.4925	1.1168	1.8105	1.4577	2.3632	2.3179	3.7576
	3	USD	0.9697	1.572	1.0523	1.7059	1.152	1.8676	1.2769	2.0701	1.4484	2.348
		UAD	0.9919	1.608	1.1425	1.8521	1.3694	2.2199	1.7736	2.8753	2.8439	4.6104
		ED	0.9965	1.6154	1.1614	1.8828	1.4088	2.2839	1.8389	2.9812	2.924	4.7403
	4	USD	1.0591	1.717	1.1492	1.863	1.2578	2.039	1.3935	2.2591	1.5791	2.5599
		UAD	1.0835	1.7564	1.2479	2.023	1.4957	2.4247	1.9374	3.1407	3.1071	5.037
		ED	1.0885	1.7646	1.2687	2.0567	1.5389	2.4948	2.0088	3.2565	3.1941	5.178

Table 5: Influence of porosity distribution and PVF on Dimensionless axial stress S_{11} in FG plate

			PVF =0.1		PVF =0.3		PVF =0.5		PVF =0.7		PVF =0.9	
a/h	b/a	Distribution	SSL	UDL	SSL	UDL	SSL	UDL	SSL	UDL	SSL	UDL
2	1	USD	0.2944	0.4772	0.3234	0.5242	0.3609	0.585	0.4139	0.6709	0.5055	0.8195
		UAD	0.2958	0.4795	0.3291	0.5336	0.3751	0.6081	0.4468	0.7243	0.6001	0.9729
		ED	0.282	0.4572	0.282	0.4572	0.282	0.4572	0.282	0.4572	0.282	0.4572
	2	USD	0.5215	0.8455	0.5708	0.9253	0.6331	1.0263	0.7181	1.1641	0.8564	1.3884
		UAD	0.5237	0.849	0.5804	0.9409	0.6586	1.0677	0.7823	1.2681	1.059	1.7167
		ED	0.5004	0.8112	0.5004	0.8112	0.5004	0.8112	0.5004	0.8112	0.5004	0.8112
	3	USD	0.6152	0.9973	0.6726	1.0903	0.7448	1.2074	0.8424	1.3656	0.9986	1.6188
		UAD	0.6177	1.0015	0.6842	1.1091	0.7757	1.2575	0.9208	1.4928	1.2477	2.0227
		ED	0.5904	0.9571	0.5904	0.9571	0.5904	0.9571	0.5904	0.9571	0.5904	0.9571
	4	USD	0.6563	1.0639	0.7173	1.1628	0.7938	1.2869	0.8969	1.454	1.0608	1.7197
		UAD	0.6591	1.0685	0.7298	1.183	0.8272	1.341	0.9817	1.5915	1.3306	2.1571
		ED	0.63	1.0213	0.63	1.0213	0.63	1.0213	0.63	1.0213	0.63	1.0213
5	1	USD	0.2182	0.3537	0.2368	0.3839	0.2593	0.4204	0.2876	0.4663	0.3267	0.5296
		UAD	0.2189	0.3549	0.2406	0.3901	0.2707	0.4388	0.3195	0.5179	0.4384	0.7108
		ED	0.21	0.3404	0.21	0.3404	0.21	0.3404	0.21	0.3404	0.21	0.3404
	2	USD	0.4471	0.7248	0.4845	0.7855	0.5294	0.8582	0.5847	0.9478	0.6577	1.0662
		UAD	0.4491	0.7281	0.4941	0.801	0.5562	0.9016	0.6564	1.0641	0.8974	1.4548
		ED	0.4305	0.6979	0.4305	0.6979	0.4305	0.6979	0.4305	0.6979	0.4305	0.6979
	3	USD	0.541	0.8771	0.5862	0.9504	0.6402	1.0378	0.7065	1.1453	0.7933	1.286
		UAD	0.5436	0.8813	0.5983	0.97	0.6737	1.0922	0.7951	1.289	1.0858	1.7602
		ED	0.521	0.8447	0.521	0.8447	0.521	0.8447	0.521	0.8447	0.521	0.8447
	4	USD	0.5823	0.944	0.6309	1.0227	0.6888	1.1167	0.7599	1.232	0.8527	1.3824
		UAD	0.5852	0.9486	0.6441	1.0442	0.7253	1.1759	0.8561	1.3878	1.1685	1.8944
		ED	0.5608	0.9091	0.5608	0.9091	0.5608	0.9091	0.5608	0.9091	0.5608	0.9091
10	1	USD	0.2083	0.3376	0.2254	0.3654	0.2457	0.3984	0.2703	0.4383	0.3014	0.4887
		UAD	0.209	0.3388	0.2292	0.3715	0.2571	0.4168	0.3028	0.4909	0.4171	0.6762
		ED	0.2007	0.3253	0.2007	0.3253	0.2007	0.3253	0.2007	0.3253	0.2007	0.3253
	2	USD	0.4373	0.7089	0.473	0.7669	0.5153	0.8354	0.5663	0.918	0.6296	1.0207
		UAD	0.4393	0.7122	0.4828	0.7826	0.5427	0.8797	0.6397	1.037	0.8758	1.4198
		ED	0.4213	0.683	0.4213	0.683	0.4213	0.683	0.4213	0.683	0.4213	0.683
	3	USD	0.5312	0.8612	0.5747	0.9316	0.626	1.0148	0.6877	1.1149	0.7643	1.239
		UAD	0.5339	0.8655	0.587	0.9516	0.6602	1.0703	0.7784	1.2619	1.0641	1.7251
		ED	0.5119	0.8299	0.5119	0.8299	0.5119	0.8299	0.5119	0.8299	0.5119	0.8299
	4	USD	0.5725	0.9281	0.6193	1.004	0.6746	1.0936	0.741	1.2013	0.8234	1.3348
		UAD	0.5754	0.9328	0.6328	1.0259	0.7118	1.154	0.8393	1.3607	1.1468	1.8591
		ED	0.5517	0.8944	0.5517	0.8944	0.5517	0.8944	0.5517	0.8944	0.5517	0.8944

Table 6: Influence of porosity distribution and PVF on dimensionless stress, S_{13} in FG plate

			PVF =0.1		PVF =0.3		PVF =0.5		PVF =0.7		PVF =0.9	
a/h	b/a	Distribution	SSL	UDL	SSL	UDL	SSL	UDL	SSL	UDL	SSL	UDL
2	1	USD	0.2288	0.3709	0.2158	0.3499	0.1963	0.3182	0.1629	0.264	0.0889	0.1442
		UAD	0.2329	0.3776	0.2305	0.3737	0.2272	0.3683	0.222	0.3599	0.2126	0.3447
		ED	0.2339	0.3791	0.2339	0.3791	0.2339	0.3791	0.2339	0.3791	0.2339	0.3791
	2	USD	0.3693	0.5988	0.3486	0.5651	0.3174	0.5145	0.2638	0.4277	0.1445	0.2343
		UAD	0.3759	0.6093	0.3721	0.6032	0.3667	0.5945	0.3585	0.5812	0.3434	0.5568
		ED	0.3774	0.6118	0.3774	0.6118	0.3774	0.6118	0.3774	0.6118	0.3774	0.6118
	3	USD	0.4162	0.6746	0.3928	0.6368	0.3577	0.5799	0.2974	0.4822	0.1631	0.2644
		UAD	0.4235	0.6865	0.4192	0.6796	0.4132	0.6699	0.404	0.6549	0.387	0.6274
		ED	0.4252	0.6893	0.4252	0.6893	0.4252	0.6893	0.4252	0.6893	0.4252	0.6893
	4	USD	0.4354	0.7059	0.411	0.6663	0.3743	0.6069	0.3113	0.5046	0.1707	0.2768
		UAD	0.4431	0.7183	0.4386	0.7111	0.4324	0.7009	0.4227	0.6852	0.405	0.6565
		ED	0.4449	0.7212	0.4449	0.7212	0.4449	0.7212	0.4449	0.7212	0.4449	0.7212
5	1	USD	0.2331	0.3779	0.2202	0.357	0.2008	0.3255	0.1672	0.2711	0.0921	0.1493
		UAD	0.2371	0.3844	0.2348	0.3806	0.2315	0.3753	0.2264	0.367	0.217	0.3517
		ED	0.2381	0.386	0.2381	0.386	0.2381	0.386	0.2381	0.386	0.2381	0.386
	2	USD	0.3734	0.6053	0.3528	0.5719	0.3217	0.5215	0.2681	0.4346	0.1477	0.2394
		UAD	0.3798	0.6158	0.3761	0.6097	0.3708	0.6011	0.3626	0.5879	0.3476	0.5635
		ED	0.3813	0.6182	0.3813	0.6182	0.3813	0.6182	0.3813	0.6182	0.3813	0.6182
	3	USD	0.4201	0.6811	0.397	0.6435	0.362	0.5869	0.3017	0.489	0.1662	0.2694
		UAD	0.4274	0.6929	0.4232	0.686	0.4172	0.6764	0.4081	0.6615	0.3911	0.6341
		ED	0.4291	0.6956	0.4291	0.6956	0.4291	0.6956	0.4291	0.6956	0.4291	0.6956
	4	USD	0.4394	0.7123	0.4152	0.673	0.3786	0.6138	0.3155	0.5115	0.1738	0.2818
		UAD	0.447	0.7246	0.4426	0.7175	0.4364	0.7074	0.4268	0.6918	0.4091	0.6632
		ED	0.4488	0.7275	0.4488	0.7275	0.4488	0.7275	0.4488	0.7275	0.4488	0.7275
10	1	USD	0.2336	0.3787	0.2208	0.3579	0.2014	0.3264	0.1678	0.2721	0.0925	0.15
		UAD	0.2377	0.3853	0.2353	0.3815	0.232	0.3761	0.2269	0.3679	0.2175	0.3526
		ED	0.2386	0.3868	0.2386	0.3868	0.2386	0.3868	0.2386	0.3868	0.2386	0.3868
	2	USD	0.3739	0.6061	0.3533	0.5728	0.3223	0.5225	0.2686	0.4355	0.1481	0.2401
		UAD	0.3804	0.6166	0.3766	0.6105	0.3713	0.602	0.3632	0.5888	0.3482	0.5644
		ED	0.3818	0.619	0.3818	0.619	0.3818	0.619	0.3818	0.619	0.3818	0.619
	3	USD	0.4207	0.682	0.3975	0.6444	0.3626	0.5878	0.3022	0.49	0.1667	0.2702
		UAD	0.4279	0.6937	0.4237	0.6869	0.4178	0.6773	0.4086	0.6624	0.3917	0.635
		ED	0.4296	0.6964	0.4296	0.6964	0.4296	0.6964	0.4296	0.6964	0.4296	0.6964
	4	USD	0.4399	0.7132	0.4157	0.6739	0.3792	0.6147	0.3161	0.5124	0.1743	0.2825
		UAD	0.4475	0.7255	0.4431	0.7183	0.4369	0.7083	0.4273	0.6927	0.4096	0.6641
		ED	0.4493	0.7283	0.4493	0.7283	0.4493	0.7283	0.4493	0.7283	0.4493	0.7283

Lastly, Figure 6 illustrates the variation of dimensionless transverse shear stress S_{13} of FG rectangular (b/a=3) in the thickness direction for a/h=5 with different values of PVF. From Figures 6a & 6b it is noted that the S_{13} increases as PVF increases. The increase of PVF results in increase of S_{13} for two types of uneven porosity distributions for both SSL and UDL. For even porosity distribution, S_{13} varies anti-symmetrically about the mid plate for all porosity volume fractions for both SSL and UDL. Also, noticed that for even porosity distribution the stress S_{13} varies only in the thickness direction and is independent of PVF. From Figures 6a-b it is noteworthy to see that the volume fraction of porosity PVF of uneven symmetrical and uneven asymmetrical distribution has no influence on transverse shear stress in two and one position respectively, are S_{13}=0.41 (SSL), 0.64 (UDL) at z/h=-0.19 & 0.19, and S_{13}=0.48 (SSL), 0.74 (UDL) at z/h=0.04. The maximum transverse shear stress for uneven symmetrical and uneven asymmetrical distribution occurs at z/h=-0.3 and 0.3 & z/h=0.2 respectively and not at the plate center for both SSL and UDL. The S_{13} varies parabolically in the thickness direction of the plate for SSL and UDL of even porosity distribution and is independent of PVF values.

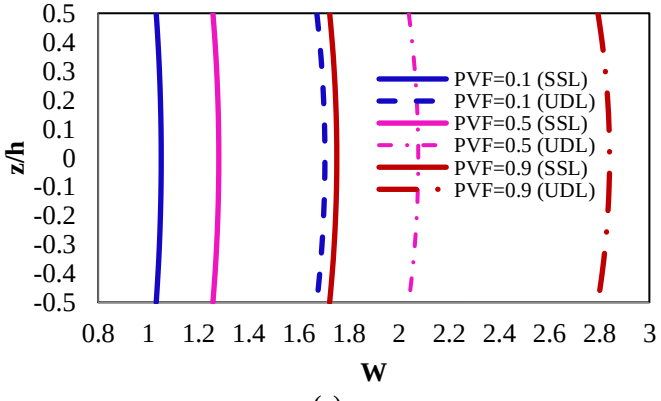

(a)

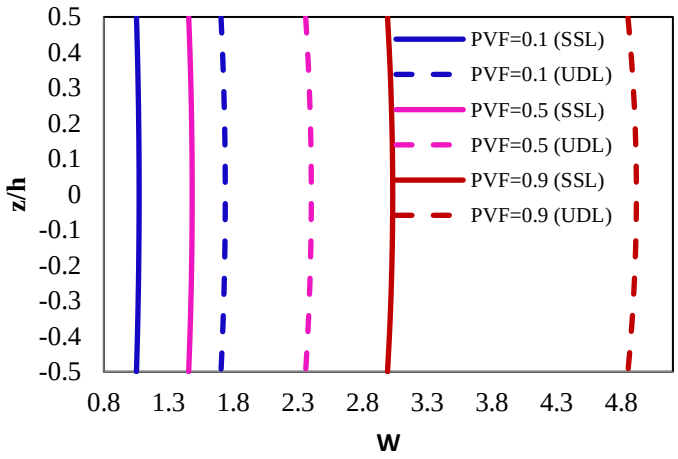

(b)

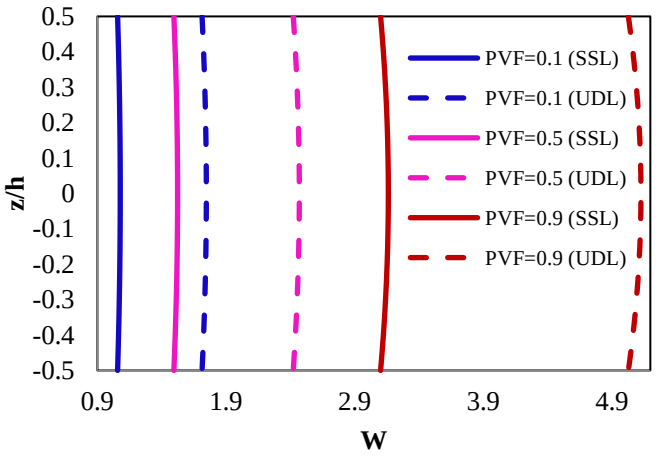

(c)

Figure. 3. Distributions of dimensionless deflection along the thickness of Rectangular (b/a=3) FG plate with (a) Uneven symmetrical distribution subjected to SSL &UDL; (b) Uneven asymmetric distribution subjected to SSL &UDL; (c) Evenly distribution subjected to SSL &UDL for a/h=5.

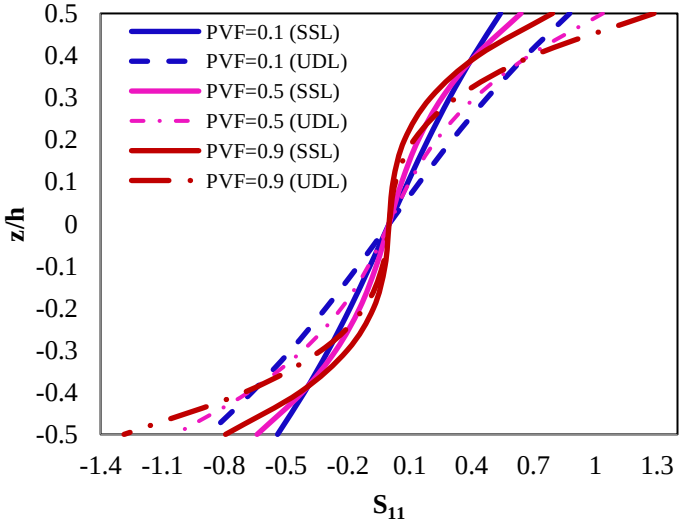

(a)

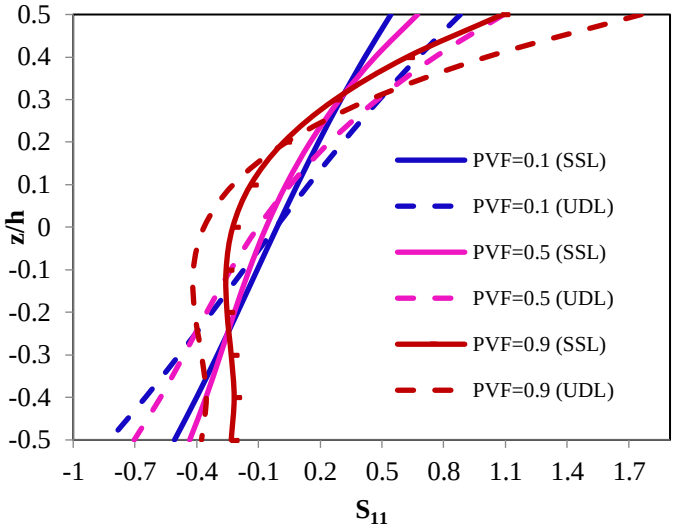

(b)

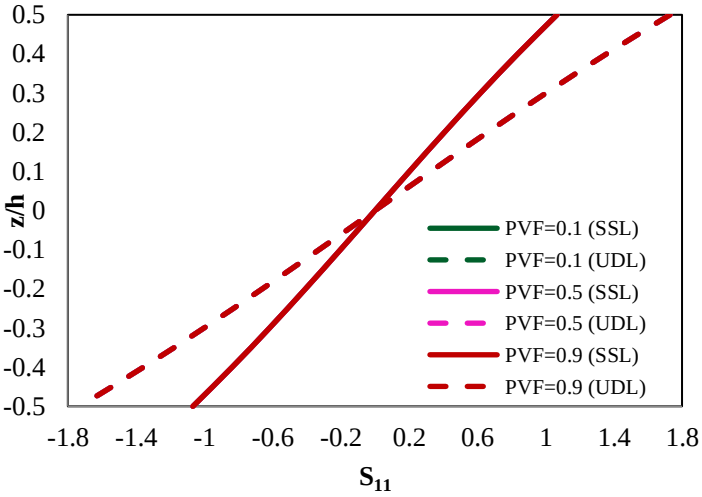

(c)

Figure. 4. Distributions of dimensionless axial stress, S_{11} along the thickness of Rectangular (b/a=3) FG plate with (a) Uneven symmetrical distribution subjected to SSL &UDL; (b) Uneven asymmetric distribution subjected to SSL &UDL; (c) Evenly distribution subjected to SSL &UDL for a/h=5.

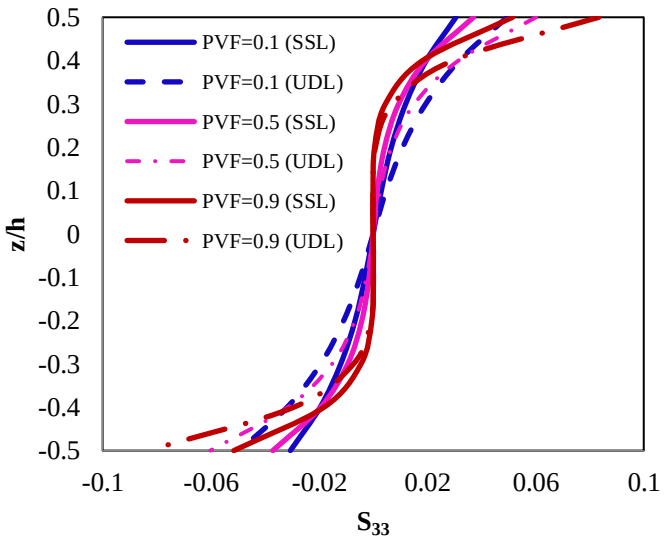

(a)

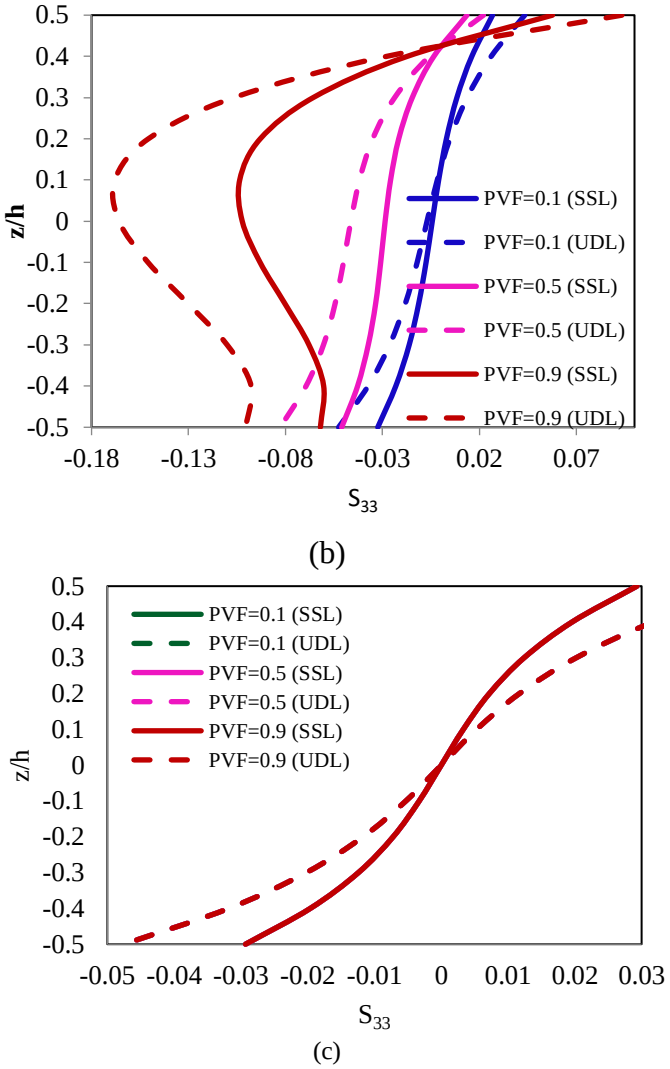

Figure. 5. Distributions of dimensionless normal stress, S_{33} along the thickness of Rectangular (b/a=3) FG plate with (a) Uneven symmetrical distribution subjected to SSL &UDL; (b) Uneven asymmetric distribution subjected to SSL &UDL; (c) Evenly distribution subjected to SSL &UDL for a/h=5.

Lastly, Figure 6 illustrates the variation of dimensionless transverse shear stress S_{13} of FG rectangular (b/a=3) in the thickness direction for a/h=5 with different values of PVF.

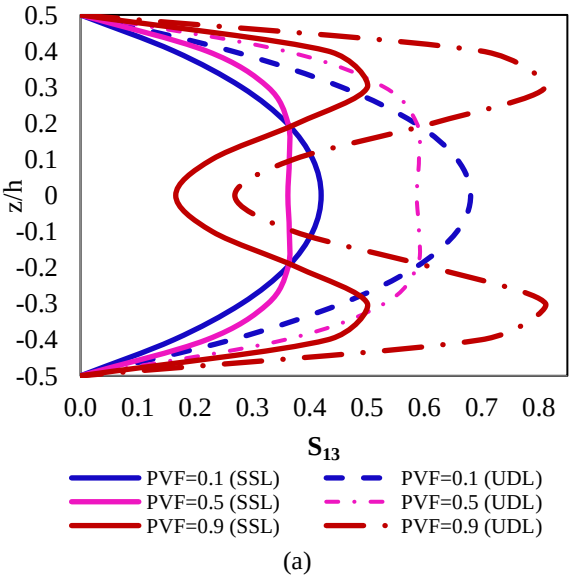

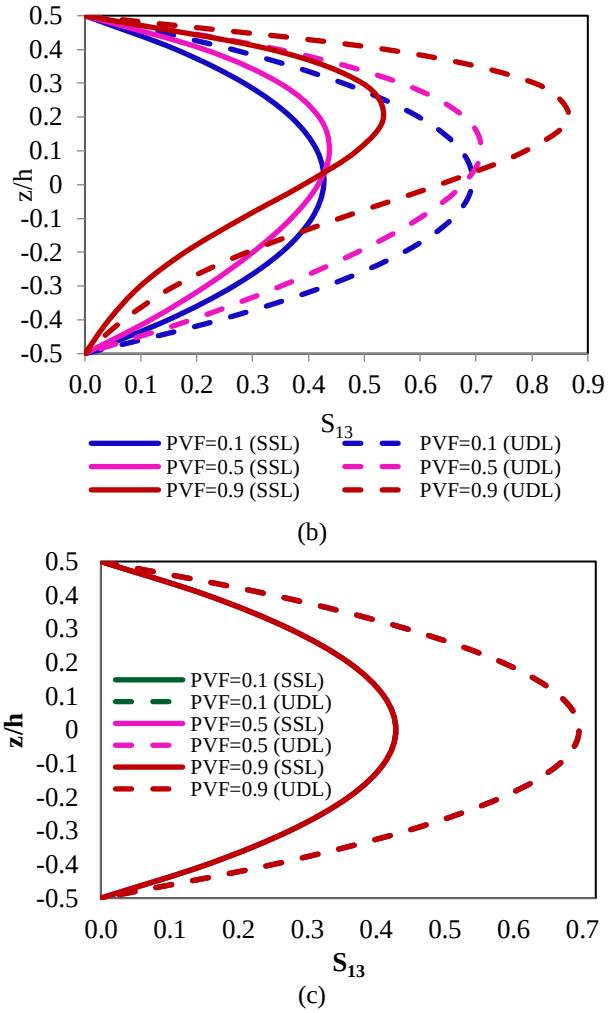

Figure. 6. Distributions of dimensionless Transverse shear stress, S_{13} along the thickness of Rectangular (b/a=3) FG plate with (a) Uneven symmetrical distribution subjected to SSL &UDL; (b) Uneven asymmetric distribution subjected to SSL &UDL; (c) Evenly distribution subjected to SSL &UDL for a/h=5.

5. Conclusions

A thickness stretching higher order displacement model with a new shear strain shape function is considered to research the single-layered FG plates with porosities subjected to both SSL and UDL. This theory fulfills the nullity of the transverse shear stresses at the top and bottom of the FG plate and thus eliminates the use of a shear correction factor. The equilibrium equations are obtained by employing the principle of virtual displacements. The even, uneven symmetrical and uneven asymmetrical porosity distributions are used to approximately portray the variations of the properties of porous FG plates. Several examples are presented to validate the present theory. The numerical results estimated by the present theory are accurate in estimating the bending response of perfect and porous FG plates. The influence of ratios of a/h, b/a, and PVF on the flexural response of porous FGPs are studied. The numerical results to the center deflections and stresses for several values of volume fraction of porosities and distributions are also reported and analyzed. From the results of the present theory, it is established that the inclusion of porosity, increases the dimensionless center deflections and axial stresses while it decreases the transverse shear stresses. Also, the even porosity distribution leads to somewhat larger deflections and transverse shear stresses compared to other two types of uneven distributions, while the axial stress is considerably lower values which could be

considered as a key factor in the optimal design of the porous FGPs. Also, the control results provided in this paper can be used to assess various plate theories and also to compare the results provided by other analytical methods and finite element methods.

References

[1] D. Chen, J. Yang, S. Kitipornchai, Free and forced vibrations of shear deformable functionally graded porous beams, *International journal of mechanical sciences*, Vol. 108, pp. 14-22, 2016.

[2] N. Wattanasakulpong, A. Chaikittiratana, S. Pornpeerakeat, Chebyshev collocation approach for vibration analysis of functionally graded porous beams based on third-order shear deformation theory, *Acta Mechanica Sinica*, Vol. 34, No. 6, pp. 1124-1135, 2018.

[3] M. Mohammadi, M. Ghayour, A. Farajpour, Analysis of free vibration sector plate based on elastic medium by using new version of differential quadrature method, *Journal of Simulation and Analysis of Novel Technologies in Mechanical Engineering*, Vol. 3, No. 2, pp. 47-56, 2010.

[4] M. Mohammadi, A. Farajpour, M. Goodarzi, H. Mohammadi, Temperature Effect on Vibration Analysis of Annular Graphene Sheet Embedded on Visco-Pasternak Foundati, *Journal of Solid Mechanics*, Vol. 5, No. 3, pp. 305-323, 2013.

[5] M. Safarabadi, M. Mohammadi, A. Farajpour, M. Goodarzi, Effect of surface energy on the vibration analysis of rotating nanobeam, 2015.

[6] M. Baghani, M. Mohammadi, A. Farajpour, Dynamic and stability analysis of the rotating nanobeam in a nonuniform magnetic field considering the surface energy, *International Journal of Applied Mechanics*, Vol. 8, No. 04, pp. 1650048, 2016.

[7] M. Goodarzi, M. Mohammadi, M. Khooran, F. Saadi, Thermo-mechanical vibration analysis of FG circular and annular nanoplate based on the visco-pasternak foundation, *Journal of Solid Mechanics*, Vol. 8, No. 4, pp. 788-805, 2016.

[8] M. Zamani Nejad, A. Rastgoo, A. Hadi, Effect of exponentially-varying properties on displacements and stresses in pressurized functionally graded thick spherical shells with using iterative technique, *Journal of Solid Mechanics*, Vol. 6, No. 4, pp. 366-377, 2014.

[9] M. Z. Nejad, A. Rastgoo, A. Hadi, Exact elasto-plastic analysis of rotating disks made of functionally graded materials, *International Journal of Engineering Science*, Vol. 85, pp. 47-57, 2014.

[10] M. Hosseini, M. Shishesaz, K. N. Tahan, A. Hadi, Stress analysis of rotating nano-disks of variable thickness made of functionally graded materials, *International Journal of Engineering Science*, Vol. 109, pp. 29-53, 2016.

[11] M. Shishesaz, M. Hosseini, K. N. Tahan, A. Hadi, Analysis of functionally graded nanodisks under thermoelastic loading based on the strain gradient theory, *Acta Mechanica*, Vol. 228, No. 12, pp. 4141-4168, 2017.

[12] M. Hosseini, M. Shishesaz, A. Hadi, Thermoelastic analysis of rotating functionally graded micro/nanodisks of variable thickness, *Thin-Walled Structures*, Vol. 134, pp. 508-523, 2019.

[13] Z. Mazarei, M. Z. Nejad, A. Hadi, Thermo-elasto-plastic analysis of thick-walled spherical pressure vessels made of functionally graded materials, *International Journal of Applied Mechanics*, Vol. 8, No. 04, pp. 1650054, 2016.

[14] M. Gharibi, M. Zamani Nejad, A. Hadi, Elastic analysis of functionally graded rotating thick cylindrical pressure vessels with exponentially-varying properties using power series method of Frobenius, *Journal of Computational Applied Mechanics*, Vol. 48, No. 1, pp. 89-98, 2017.

[15] M. Zamani Nejad, M. Jabbari, A. Hadi, A review of functionally graded thick cylindrical and conical shells, *Journal of Computational Applied Mechanics*, Vol. 48, No. 2, pp. 357-370, 2017.

[16] A. Hadi, A. Rastgoo, N. Haghighipour, A. Bolhassani, Numerical modelling of a spheroid living cell membrane under hydrostatic pressure, *Journal of Statistical Mechanics: Theory and Experiment*, Vol. 2018, No. 8, pp. 083501, 2018.

[17] M. Z. Nejad, N. Alamzadeh, A. Hadi, Thermoelastoplastic analysis of FGM rotating thick cylindrical pressure vessels in linear elastic-fully plastic condition, *Composites Part B: Engineering*, Vol. 154, pp. 410-422, 2018.

[18] B. Karami, D. Shahsavari, M. Janghorban, L. Li, On the resonance of functionally graded nanoplates using bi-Helmholtz nonlocal strain gradient theory, *International Journal of Engineering Science*, Vol. 144, pp. 103143, 2019.

[19] E. Zarezadeh, V. Hosseini, A. Hadi, Torsional vibration of functionally graded nano-rod under magnetic field supported by a generalized torsional foundation based on nonlocal elasticity theory, *Mechanics Based Design of Structures and Machines*, Vol. 48, No. 4, pp. 480-495, 2020.

[20] A. Farajpour, M. Danesh, M. Mohammadi, Buckling analysis of variable thickness nanoplates using nonlocal continuum mechanics, *Physica E: Low-dimensional Systems and Nanostructures*, Vol. 44, No. 3, pp. 719-727, 2011.

[21] A. Farajpour, M. Mohammadi, A. Shahidi, M. Mahzoon, Axisymmetric buckling of the circular graphene sheets with the nonlocal continuum plate model, *Physica E: Low-dimensional Systems and Nanostructures*, Vol. 43, No. 10, pp. 1820-1825, 2011.

[22] A. Farajpour, A. Shahidi, M. Mohammadi, M. Mahzoon, Buckling of orthotropic micro/nanoscale plates under linearly varying in-plane load via nonlocal continuum mechanics, *Composite Structures*, Vol. 94, No. 5, pp. 1605-1615, 2012.

[23] N. GHAYOUR, A. Sedaghat, M. Mohammadi, Wave propagation approach to fluid filled submerged visco-elastic finite cylindrical shells, 2011.

[24] H. Moosavi, M. Mohammadi, A. Farajpour, S. Shahidi, Vibration analysis of nanorings using nonlocal continuum mechanics and shear deformable ring theory, *Physica E: Low-dimensional Systems and Nanostructures*, Vol. 44, No. 1, pp. 135-140, 2011.

[25] M. Danesh, A. Farajpour, M. Mohammadi, Axial vibration analysis of a tapered nanorod based on nonlocal elasticity theory and differential quadrature method, *Mechanics Research Communications*, Vol. 39, No. 1, pp. 23-27, 2012.

[26] M. Mohammadi, M. Goodarzi, M. Ghayour, S. Alivand, Small scale effect on the vibration of orthotropic plates

embedded in an elastic medium and under biaxial in-plane pre-load via nonlocal elasticity theory, 2012.

[27] M. Goodarzi, M. Mohammadi, A. Farajpour, M. Khooran, Investigation of the effect of pre-stressed on vibration frequency of rectangular nanoplate based on a visco-Pasternak foundation, 2014.

[28] M. Mohammadi, A. Farajpour, M. Goodarzi, Numerical study of the effect of shear in-plane load on the vibration analysis of graphene sheet embedded in an elastic medium, *Computational Materials Science*, Vol. 82, pp. 510-520, 2014.

[29] M. Mohammadi, A. Farajpour, M. Goodarzi, R. Heydarshenas, Levy type solution for nonlocal thermo-mechanical vibration of orthotropic mono-layer graphene sheet embedded in an elastic medium, *Journal of Solid Mechanics*, Vol. 5, No. 2, pp. 116-132, 2013.

[30] M. Mohammadi, A. Farajpour, M. Goodarzi, F. Dinari, Thermo-mechanical vibration analysis of annular and circular graphene sheet embedded in an elastic medium, *Latin American Journal of Solids and Structures*, Vol. 11, No. 4, pp. 659-682, 2014.

[31] M. Mohammadi, A. Moradi, M. Ghayour, A. Farajpour, Exact solution for thermo-mechanical vibration of orthotropic mono-layer graphene sheet embedded in an elastic medium, *Latin American Journal of Solids and Structures*, Vol. 11, No. 3, pp. 437-458, 2014.

[32] M. Mohammadi, M. Ghayour, A. Farajpour, Free transverse vibration analysis of circular and annular graphene sheets with various boundary conditions using the nonlocal continuum plate model, *Composites Part B: Engineering*, Vol. 45, No. 1, pp. 32-42, 2013.

[33] M. Mohammadi, M. Goodarzi, M. Ghayour, A. Farajpour, Influence of in-plane pre-load on the vibration frequency of circular graphene sheet via nonlocal continuum theory, *Composites Part B: Engineering*, Vol. 51, pp. 121-129, 2013.

[34] S. Asemi, A. Farajpour, H. Asemi, M. Mohammadi, Influence of initial stress on the vibration of double-piezoelectric-nanoplate systems with various boundary conditions using DQM, *Physica E: Low-dimensional Systems and Nanostructures*, Vol. 63, pp. 169-179, 2014.

[35] S. Asemi, A. Farajpour, M. Mohammadi, Nonlinear vibration analysis of piezoelectric nanoelectromechanical resonators based on nonlocal elasticity theory, *Composite Structures*, Vol. 116, pp. 703-712, 2014.

[36] S. R. Asemi, M. Mohammadi, A. Farajpour, A study on the nonlinear stability of orthotropic single-layered graphene sheet based on nonlocal elasticity theory, *Latin American Journal of Solids and Structures*, Vol. 11, No. 9, pp. 1515-1540, 2014.

[37] M. Mohammadi, A. Farajpour, A. Moradi, M. Ghayour, Shear buckling of orthotropic rectangular graphene sheet embedded in an elastic medium in thermal environment, *Composites Part B: Engineering*, Vol. 56, pp. 629-637, 2014.

[38] A. Farajpour, A. Rastgoo, M. Mohammadi, Surface effects on the mechanical characteristics of microtubule networks in living cells, *Mechanics Research Communications*, Vol. 57, pp. 18-26, 2014.

[39] A. Farajpour, A. Rastgoo, M. Mohammadi, Vibration, buckling and smart control of microtubules using piezoelectric nanoshells under electric voltage in thermal environment, *Physica B: Condensed Matter*, Vol. 509, pp. 100-114, 2017.

[40] H. Asemi, S. Asemi, A. Farajpour, M. Mohammadi, Nanoscale mass detection based on vibrating piezoelectric ultrathin films under thermo-electro-mechanical loads, *Physica E: Low-dimensional Systems and Nanostructures*, Vol. 68, pp. 112-122, 2015.

[41] A. Farajpour, M. H. Yazdi, A. Rastgoo, M. Loghmani, M. Mohammadi, Nonlocal nonlinear plate model for large amplitude vibration of magneto-electro-elastic nanoplates, *Composite Structures*, Vol. 140, pp. 323-336, 2016.

[42] A. Farajpour, M. H. Yazdi, A. Rastgoo, M. Mohammadi, A higher-order nonlocal strain gradient plate model for buckling of orthotropic nanoplates in thermal environment, *Acta Mechanica*, Vol. 227, No. 7, pp. 1849-1867, 2016.

[43] M. R. Farajpour, A. Rastgoo, A. Farajpour, M. Mohammadi, Vibration of piezoelectric nanofilm-based electromechanical sensors via higher-order non-local strain gradient theory, *Micro & Nano Letters*, Vol. 11, No. 6, pp. 302-307, 2016.

[44] M. Mohammadi, M. Safarabadi, A. Rastgoo, A. Farajpour, Hygro-mechanical vibration analysis of a rotating viscoelastic nanobeam embedded in a visco-Pasternak elastic medium and in a nonlinear thermal environment, *Acta Mechanica*, Vol. 227, No. 8, pp. 2207-2232, 2016.

[45] M. Mohammadi, A. Rastgoo, Primary and secondary resonance analysis of FG/lipid nanoplate with considering porosity distribution based on a nonlinear elastic medium, *Mechanics of Advanced Materials and Structures*, pp. 1-22, 2018.

[46] M. Mohammadi, A. Rastgoo, Nonlinear vibration analysis of the viscoelastic composite nanoplate with three directionally imperfect porous FG core, *Structural Engineering and Mechanics*, Vol. 69, No. 2, pp. 131, 2019.

[47] M. Mohammadi, M. Hosseini, M. Shishesaz, A. Hadi, A. Rastgoo, Primary and secondary resonance analysis of porous functionally graded nanobeam resting on a nonlinear foundation subjected to mechanical and electrical loads, *European Journal of Mechanics-A/Solids*, Vol. 77, pp. 103793, 2019.

[48] B. S. Reddy, J. S. Kumar, C. E. Reddy, K. Reddy, Buckling analysis of functionally graded material plates using higher order shear deformation theory, *Journal of composites*, Vol. 2013, 2013.

[49] B. S. Redddy, J. S. Kumar, C. E. Reddy, K. V. K. Reddy, Free vibration behaviour of functionally graded plates using higher-order shear deformation theory, *Journal of Applied Science and Engineering*, Vol. 17, No. 3, pp. 231-241, 2014.

[50] B. SiddaRedddy, J. S. Kumar, C. EswaraReddy, K. Reddy, Static Bending Behavior of Functionally Graded Plates Subjected to Mechanical Loading, *Jordan Journal of Mechanical & Industrial Engineering*, Vol. 8, No. 4, 2014.

[51] B. S. Reddy, J. S. Kumar, C. Reddy, K. V. K. Reddy, Buckling analysis of functionally graded plates using higher order shear deformation theory with thickness stretching effect, *International Journal of Applied Science and Engineering*, Vol. 13, No. 1, pp. 19-36, 2015.

[52] S. R. Bathini, Thermomechanical behaviour of Functionally Graded Plates with HSDT, *Journal of Computational & Applied Research in Mechanical Engineering (JCARME)*, 2019.

[53] B. S. Reddy, Bending Behaviour Of Exponentially Graded Material Plates Using New Higher Order Shear Deformation Theory with Stretching Effect, *International Journal of Engineering Research*, Vol. 3, pp. 124-131, 2014.

[54] B. S. Reddy, A. R. Reddy, J. S. Kumar, K. V. K. Reddy, Bending analysis of laminated composite plates using finite element method, *International journal of engineering, science and technology*, Vol. 4, No. 2, pp. 177-190, 2012.

[55] J. S. Kumar, B. S. Reddy, C. E. Reddy, K. V. K. Reddy, Geometrically non linear analysis of functionally graded material plates using higher order theory, *International Journal of Engineering, Science and Technology*, Vol. 3, No. 1, 2011.

[56] K. Suresh, S. R. Jyothula, E. R. Bathini, K. Vijaya, Nonlinear thermal analysis of functionally graded plates using higher order theory, *Innovative Systems Design and Engineering*, Vol. 2, No. 5, pp. 1-13, 2011.

[57] A. M. Zenkour, A quasi-3D refined theory for functionally graded single-layered and sandwich plates with porosities, *Composite Structures*, Vol. 201, pp. 38-48, 2018.

[58] S. Merdaci, H. Belghoul, High-order shear theory for static analysis of functionally graded plates with porosities, *Comptes Rendus Mécanique*, Vol. 347, No. 3, pp. 207-217, 2019.

[59] J. Zhao, Q. Wang, X. Deng, K. Choe, R. Zhong, C. Shuai, Free vibrations of functionally graded porous rectangular plate with uniform elastic boundary conditions, *Composites Part B: Engineering*, Vol. 168, pp. 106-120, 2019.

[60] Ş. D. Akbaş, Vibration and static analysis of functionally graded porous plates, *Journal of Applied and Computational Mechanics*, Vol. 3, No. 3, pp. 199-207, 2017.

[61] N. V. Nguyen, H. X. Nguyen, S. Lee, H. Nguyen-Xuan, Geometrically nonlinear polygonal finite element analysis of functionally graded porous plates, *Advances in Engineering Software*, Vol. 126, pp. 110-126, 2018.

[62] K. Li, D. Wu, X. Chen, J. Cheng, Z. Liu, W. Gao, M. Liu, Isogeometric analysis of functionally graded porous plates reinforced by graphene platelets, *Composite Structures*, Vol. 204, pp. 114-130, 2018.

[63] M. Slimane, Analysis of Bending of Ceramic-Metal Functionally Graded Plates with Porosities Using of High Order Shear Theory, in *Proceeding of*.

[64] P. A. Demirhan, V. Taskin, Bending and free vibration analysis of Levy-type porous functionally graded plate using state space approach, *Composites Part B: Engineering*, Vol. 160, pp. 661-676, 2019.

[65] S. Coskun, J. Kim, H. Toutanji, Bending, free vibration, and buckling analysis of functionally graded porous micro-plates using a general third-order plate theory, *Journal of Composites Science*, Vol. 3, No. 1, pp. 15, 2019.

[66] J. Kim, K. K. Żur, J. Reddy, Bending, free vibration, and buckling of modified couples stress-based functionally graded porous micro-plates, *Composite Structures*, Vol. 209, pp. 879-888, 2019.

[67] D. Chen, J. Yang, S. Kitipornchai, Buckling and bending analyses of a novel functionally graded porous plate using Chebyshev-Ritz method, *Archives of Civil and Mechanical Engineering*, Vol. 19, No. 1, pp. 157-170, 2019.

[68] A. A. Daikh, A. M. Zenkour, Effect of porosity on the bending analysis of various functionally graded sandwich plates, *Materials Research Express*, Vol. 6, No. 6, pp. 065703, 2019.

[69] A. Farzam, B. Hassani, Isogeometric analysis of in-plane functionally graded porous microplates using modified couple stress theory, *Aerospace Science and Technology*, Vol. 91, pp. 508-524, 2019.

[70] S. Bathini, K. Vijaya Kumar Reddy, Flexural behavior of porous functionally graded plates using a novel higher order theory, *Journal of Computational Applied Mechanics*, 2020.

[71] A. Zenkour, Benchmark trigonometric and 3-D elasticity solutions for an exponentially graded thick rectangular plate, *Archive of Applied Mechanics*, Vol. 77, No. 4, pp. 197-214, 2007.

[72] J. Mantari, C. G. Soares, A novel higher-order shear deformation theory with stretching effect for functionally graded plates, *Composites Part B: Engineering*, Vol. 45, No. 1, pp. 268-281, 2013.

[73] J. Mantari, C. G. Soares, Bending analysis of thick exponentially graded plates using a new trigonometric higher order shear deformation theory, *Composite Structures*, Vol. 94, No. 6, pp. 1991-2000, 2012.